南京航空航天大学

论 文 集

（一九九九年）

第2册

（一系）

南京航空航天大学科技部编

二〇〇〇年三月

一　　系

目　录

一〇三教研室(61篇)上

Proceedings of the
1999 ASME Design Engineering Technical Conferences
September 12-15, 1999, Las Vegas, Nevada

IDENTIFICATION OF IMPACT DAMPING OF TWO ELASTIC BODIES

Haiyan Hu
Nanjing University of Aeronautics and Astronautics,
Institute of Vibration Engineering Research,
Nanjing 210016, P. R .China
E-mail: hhyae@dns.nuaa.edu.cn

Dongping Jin
Nanjing University of Aeronautics and Astronautics,
Institute of Vibration Engineering Research,
Nanjing 210016, P. R. China
E-mail: jindp@dns.nuaa.edu.cn

KEY WORDS: identification, impact-vibration, elastic body, experiment

ABSTRACT

The contact force of two impacting elastic bodies is widely modeled as the parallel combination of a nonlinear spring and a nonlinear dashpot. The restoring force of the nonlinear spring can be determined according to the Hertzian contact law in elasticity, while the model and corresponding parameters of the nonlinear damping force have to be identified through experiments. The current approaches of damping identification are based on the measured time histories of both contact force and relative approaching velocity of two impacting bodies. In this paper, a new technique is presented for the damping identification on the basis of measured time history of the contact force only. Hence, the tough problem of measuring the relative approaching velocity of two impacting bodies just before impact is removed. The efficacy test of the new technique is given in the paper through an example of identifying the impact damping of a pair of clamped beams.

1 INTRODUCTION

Unavoidable clearances exist in the space structure composed of elastic rods and beams so that the vibro-impacts between the flexible components occur when the structure is subject to any environmental disturbance. It is essential to model the dynamic contact force of two elastic components in the impact phase before any theoretical or numerical analysis is made for the structural dynamics.

In the early study of modeling the dynamic contact force, Dubowsky and Gardner (1975) used the linear model of a spring and a dashpot. They found in the numerical simulations that the damping force was not equal to zero at the initial impact moment and the recovering force was negative after the impact. These numerical results deviated from the experimental ones because the dynamic contact force was overly simplified to a linear function of deformation and its velocity.

In general, the dynamic contact force F includes the elastic force and damping force as follows

$$F = k_0 u^n + D\dot{u}\,, \tag{1}$$

where $n = 3/2$, k_0 is the stiffness coefficient determined from the Hertzian contact law (Goldsmith, 1960), u is the relative normal deformation of the contact points of the two elastic bodies, and D is called damping function. A widely used damping function suggested by Hunt and Grossley (1975) takes the form

$$D = \mu_0 u^n\,, \tag{2}$$

where the parameter μ_0 is called the damping factor and should be determined through experiments. This damping model has been used by many researchers. e.g., Yigit and his co-workers (Yigit et. al., 1990 and Yigit 1994) used this model to predict the behavior of a rotating beam colliding transversally with a fixed surface. Other damping functions

may take more or less complicated forms like those suggested by Lee and Wang (1983).

In principle, the damping factor μ_0 can be identified if the time histories of F and u in Eqs. (1) and (2) are measured. However, it is not easy to measure u because it is the relative normal deformation in a tiny zone of contact. Hunt and Grossley (1975) solved this problem through the use of the coefficient of restitution denoted by e. In their technique, the coefficient of restitution e is expressed as a polynomial of V_c, the relative approaching velocity of two bodies just ahead of impact, and then a relationship between the coefficient of restitution e and the damping factor μ_0 is derived. Lankarani and Nikraveshin (1994) solved the problem from the consideration of the energy loss during the impact and found that the damping factor yields

$$\mu_0 = \frac{3k_0(1-e^2)}{4V_c}. \tag{3}$$

In these approaches, it is necessary to measure the relative approaching velocity V_c just ahead of impact. This is undoubtedly a tough problem because the relative velocity of two impacting bodies greatly changes within an extremely short duration of order 10^{-4}s.

This paper aims at developing a new approach of identifying the damping coefficient through the use of measured time history of the impact force only. For brevity, the idea behind the new approach is elucidated through the identification of impact damping of a pair of clamped beams, though it is quite straightforward to extend this approach to the identification of impact damping of more complicated elastic bodies.

2 DESCRIPTION OF IMPACTING BEAMS

Consider a pair of impacting beams shown in Fig. 1. The system of concern yields the Equation of motion

$$\begin{aligned}&\left[\rho_i A_i + M_i\delta(x-x_c)\right]\frac{\partial^2 w_i}{\partial t^2} + C_i\frac{\partial w_i}{\partial t}\\ &+D_i\frac{\partial^4 w_i}{\partial x^4} \pm F\delta(x-x_c) = 0, \quad i = 1,2,\end{aligned} \tag{4}$$

where $\rho_i A_i$ is the mass per unit length of beam i, M_i the lumped mass at beam i, C_i and D_i the coefficients of viscous damping and elastic stiffness of beam i, $w_i(x,t)$ the transverse displacement of beam i, x_c the impact position measured along the beam from the fixed end, $\delta(x)$ the Dirac function, $F(t)$ the contact force during the impact.

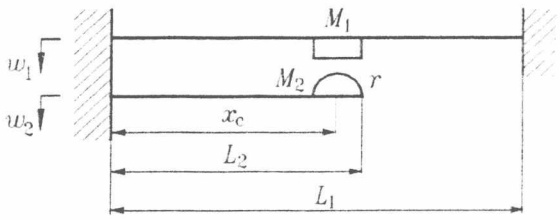

Figure 1. A pair of impacting elastic beams

To simplify the expression of the final results, a set of dimensionless variables and parameters are defined as follows

$$\begin{cases}\tau \equiv \omega t, & y \equiv \dfrac{x}{L}, & \ell \equiv \dfrac{x_c}{L},\\ \alpha \equiv \dfrac{\rho_1 A_1 D_2}{\rho_2 A_2 D_1}, & \beta \equiv \dfrac{\rho_1 A_1}{\rho_2 A_2}, & f \equiv \dfrac{FL^2}{D_1},\\ z_i \equiv \dfrac{w_i}{L}, & m_i \equiv \dfrac{M_i}{\rho_i A_i L}, & c_i \equiv \dfrac{C_i}{\rho_i A_i \omega_1},\\ i = 1,2,\end{cases} \tag{5}$$

where $\omega \equiv \sqrt{D_1/\rho_1 A_1 L^4}$, and then the dimensionless form of Eq. (5) can be derived

$$\begin{cases}\left[1+m_1\delta(y-\ell)\right]\dfrac{\partial^2 z_1}{\partial\tau^2} + c_1\dfrac{\partial z_1}{\partial\tau} + \dfrac{\partial^4 z_1}{\partial y^4}\\ +f\,\delta(y-\ell) = 0,\\ \left[1+m_2\delta(y-\ell)\right]\dfrac{\partial^2 z_2}{\partial\tau^2} + c_2\dfrac{\partial z_2}{\partial\tau} + \alpha\dfrac{\partial^4 z_2}{\partial y^4}\\ -\beta f\,\delta(y-\ell) = 0.\end{cases} \tag{6}$$

According to the Galerkin approach, $z_i(y,\tau)$ can be approximated by

$$z_i(y,\tau) = \sum_{j=1}^{N}\frac{\varphi_{ij}(y)}{\varphi_{ij}(\ell)}q_{ij}(\tau), \quad i = 1,2, \tag{7}$$

where $q_{ij}(\tau)$ is the j-th modal displacement of the i-th beam, $\varphi_{ij}(y)$ is chosen as the mode shape that yields

$$\begin{aligned}&\varphi_{ij}''''(y) - \omega_{ij}^2\left[1+m_i\delta(y-\ell)\right]\varphi_{ij}(y) = 0,\\ &j = 1,2,\ldots,N, \qquad i = 1,2,\end{aligned} \tag{8}$$

in which the primes represent the derivatives with respect to y. $\varphi_{ij}(y)$ can be determined according to the boundary conditions of the beams and scaled as

$$\int_0^1 \varphi_{ij}^2(y)\,dy = 1. \tag{9}$$

Substituting Eq. (7) into Eq. (6), integrating it with respect to x over the length of the beams, and using Eq. (9) as well as the orthogonality property of the mode shapes, one obtains

$$\begin{cases} m_{1j}\ddot{q}_{1j}(\tau)+c_{1j}\dot{q}_{1j}(\tau)+m_{1j}\omega_{1j}^2 q_{1j}(\tau) \\ +f(\tau)=0, \\ m_{2j}\ddot{q}_{2j}(\tau)+c_{2j}\dot{q}_{2j}(\tau)+\alpha m_{2j}\omega_{2j}^2 q_{2j}(\tau) \\ -\beta f(\tau)=0, \quad j=1,\ldots,N, \end{cases} \tag{10}$$

where

$$m_{ij}\equiv m_i+\frac{1}{\varphi_{ij}^2(\ell)}, \quad c_{ij}\equiv\frac{c_i}{\varphi_{ij}^2(\ell)}, \tag{11}$$
$$i=1,2, \quad j=1,\ldots,N$$

whereas the dot over q_{ij} represents the derivative with respect to τ.

It is well known that the displacements of two beams can not change within the infinitely short duration of the impact. Hence, the second and the third terms in Eq. (10) are zero when Eq. (10) is integrated over the impact duration, namely

$$\begin{cases} m_{1j}(\dot{q}_{1j}^+-\dot{q}_{1j}^-)+J=0, \\ m_{2j}(\dot{q}_{2j}^+-\dot{q}_{2j}^-)-\beta J=0, \qquad j=1,\ldots,N, \end{cases} \tag{12}$$

where $\dot{q}_{ij}^-$ and $\dot{q}_{ij}^+$ represent the j-th modal velocities of the i-th beam just before and after impact respectively, and

$$J\equiv\int_{\tau^-}^{\tau^+} f(\tau)d\tau \tag{13}$$

is the impulse of the impact force.

In practice, the coefficient of restitution e is widely used to describe the energy dissipated during the impact. It can be defined as a ratio of the relative departing velocity to the relative approaching velocity

$$e\equiv-\frac{\dot{z}_1(\ell,\tau^+)-\dot{z}_2(\ell,\tau^+)}{\dot{z}_1(\ell,\tau^-)-\dot{z}_2(\ell,\tau^-)}. \tag{14}$$

From Eq. (7), Eq. (14) can be re-written as

$$e=-\frac{\sum_{j=1}^{N}\dot{q}_{1j}^+-\sum_{j=1}^{N}\dot{q}_{2j}^+}{\sum_{j=1}^{N}\dot{q}_{1j}^--\sum_{j=1}^{N}\dot{q}_{2j}^-}. \tag{15}$$

Substituting Eq. (12) into Eq. (15) yields

$$e=\frac{J\lambda}{v_c}-1, \tag{16}$$

where

$$\lambda\equiv\sum_{j=1}^{N}\left(\frac{1}{m_{1j}}+\frac{\beta}{m_{2j}}\right), \tag{17}$$

v_c is the dimensionless relative approaching velocity of two beams at contact points just before the impact

$$v_c\equiv\dot{z}_1(\ell,\tau^-)-\dot{z}_2(\ell,\tau^-)=\sum_{j=1}^{N}\dot{q}_{1j}^--\sum_{j=1}^{N}\dot{q}_{2j}^-. \tag{18}$$

3 DETERMINATION OF DAMPING FACTOR

To identify the damping factor in Eq. (2), one can look at the equivalent form of Eq. (3) for the dimensionless displacements

$$\mu=\frac{3k(1-e^2)}{4v_c}, \tag{19}$$

where

$$\mu\equiv\frac{\mu_0\omega L^{n+3}}{D_1}, \quad k\equiv\frac{k_0L^{n+2}}{D_1}, \quad v_c=\frac{V_c}{\omega L}. \tag{20}$$

Substituting Eq. (16) into Eq. (19), one obtains a relation between μ and (v_c, J). To eliminate v_c in this relation, it is helpful to consider the relative motion of two beams during the impact. From Eqs. (7), (10) and (17), it is easy to derive the equation of the relative motion

$$\ddot{u}=-\lambda\left(ku^n+\mu u^n\dot{u}\right). \tag{21}$$

Substituting the approximate expression of $\dot{u}$ in (Hunt and Crossley, 1975) into Eq. (21) and integrating it with respect to u from zero to u_m, the maximal indentation shown in Fig. 2, one has

$$-\frac{1}{2}v_c^2\approx-\lambda\left(k\frac{u_m^{n+1}}{n+1}+\frac{\mu}{3k}v_c^3\right). \tag{22}$$

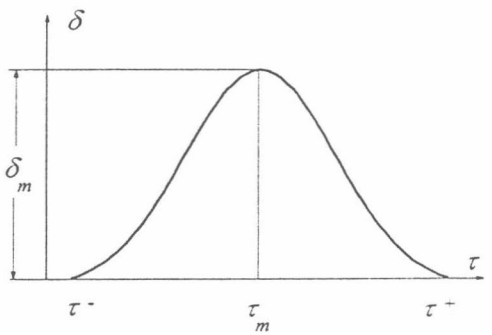

Figure 2. A typical time history of indentation

In addition, the Hertzian contact law gives the maximal dynamic contact force

$$f_m = k u_m^n \tag{23}$$

Substituting Eqs. (16), (19) and (23) into Eq. (22) yields

$$v_c^2 - J\lambda^2 v_c + 2\lambda\left[\left(\frac{J\lambda}{2}\right)^2 - \frac{k(f_m/k)^{n+1/n}}{n+1}\right] = 0 . \tag{24}$$

By substituting v_c solved from Eq. (24) into Eq. (16), one obtains the coefficient of restitution

$$e = \frac{2}{\lambda \pm \sqrt{\lambda^2 - 2\lambda + \gamma}} - 1 , \tag{25}$$

where

$$\gamma \equiv \frac{8k(f_m/k)^{n+1/n}}{(n+1)J^2\lambda} . \tag{26}$$

Equation (25) implies that the coefficient of restitution e depends on both the impulse J and the maximal impact force f_m. The effect of J and f_m on e in a typical case is shown in Fig. 3, where e keeps almost unchanged in two regions and undergoes a step between the two regions. Hence, the widely used assumption that the coefficient of restitution e is a constant holds true only in these two regions.

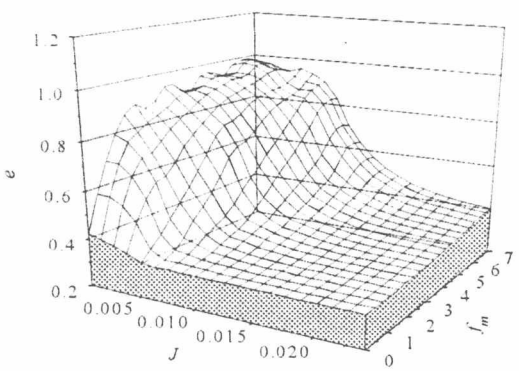

Figure 3. Coefficient of restitution versus impulse and maximal impact force

In summary, one can determine the relative approaching velocity v_c just ahead of impact and the coefficient of restitution e from the impulse J and the maximal impact force f_m, which can easily be extracted from the measured time history of the impact force. Then, one obtains the dimensionless damping factor μ from Eq. (19). Moreover, if the impact force is recorded in a test of vibro-impacts, a number of maximal values of impact force and corresponding impulses can be extracted from the record such that a series of pairs (e_k, v_{ck}), $k = 1,\ldots,m$ can be determined from Eqs. (25) and (24), so can be the function μ in e and v_c. If a constant μ is preferable to simplify the analysis in practice, it can be estimated as following

$$\mu = \frac{3k\sum_{k=1}^{m} v_{ck}(1-e_k^2)}{4\sum_{k=1}^{m} v_{ck}^2} \tag{27}$$

from (e_k, v_{ck}), $k = 1,\ldots,m$ by fitting Eq. (19) in the sense of the least squared approximation.

4 EXPERIMENTS

To check the validity of the new approach, the impact test of a pair of clamped beams shown in Fig. 4 was studied. The beams were made of the same steel and each of them was attached with a semi-spherical impact head made of steel, respectively. The length L of beams was 0.3m, the width and the thickness of beams were 0.03m and 0.00075m, respectively. The distance H between two beams was set as 0.04m. The radius of the semi-spherical impact head was 0.015m. The dynamic contact force during impact was sensed by a force transducer with the mass 0.0322kg. The clearance between the impact head of the left beam and the force transducer mounted on the right beam was 0.005m. Before the test of impact damping identification, the modal test for beams without impact was made. It was found that the vibration of each beam was dominated by the fundamental mode of 2.95Hz and the first order modal damping of single beam was about 0.2Ns/m.

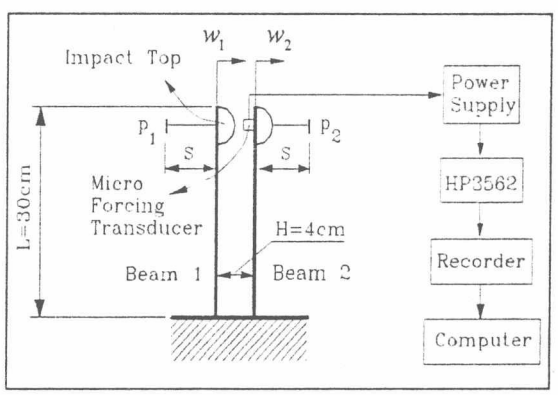

Figure 4. A schematic of experiment setup

The first test is to measure the time history of the impact force. The tips of two beams were moved to arbitrary positions and released all of a sudden so that the free vibro-impacts occurred. The impact force was recorded as shown in Fig. 5.

where the first record is the time history when the sampling frequency was set to 200Hz and the second is the case of 400Hz, respectively. From these records, the relationship between the impulse and the maximal impact force was computed as shown in Fig. 6.

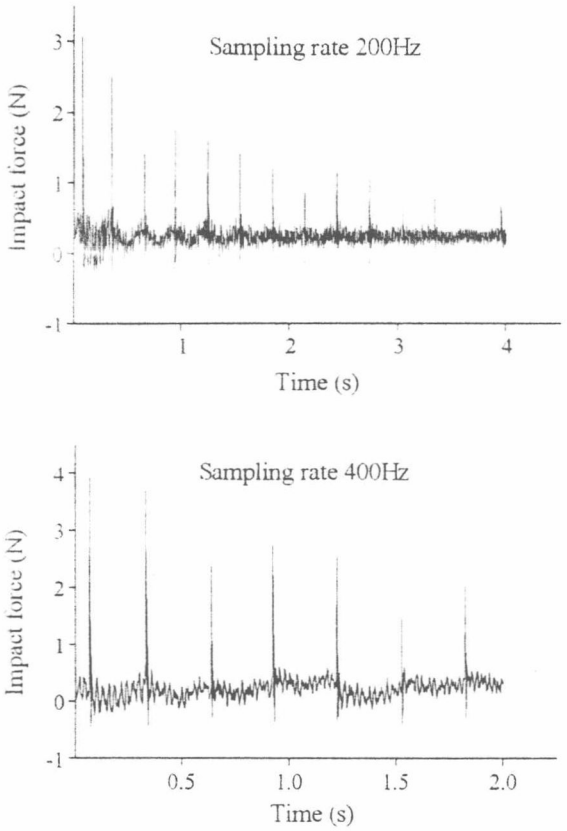

Figure 5. Measured contact force during vibro-impacts

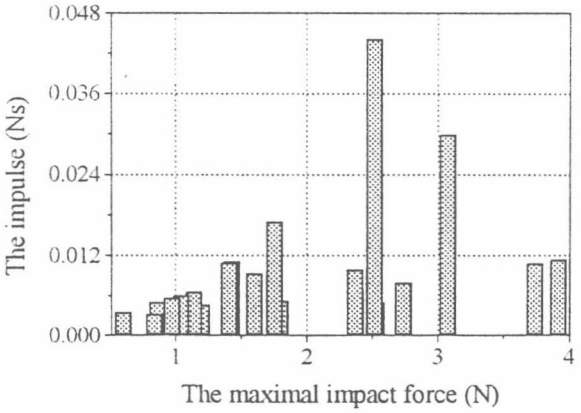

Figure 6. Experimental data: the impulse versus the maximal impact force

From the experimental data in Fig. 6, the impulse J and the maximal impact force f_m were evaluated. Then, they were substituted into Eqs. (25) and (24) so that a relationship between the coefficient of restitution e and the relative approaching velocity v_c was obtained as shown in Fig. 7. Here, e keeps almost unchanged with variation of v_c. By means of the nonlinear least squares technique, one can fit the experimental data and get $e = 0.33377 v_c^{-0.00079}$. Substituting this expression into Eq. (19), one obtains the dimensionless impact damping factor as illustrated in Fig. 8.

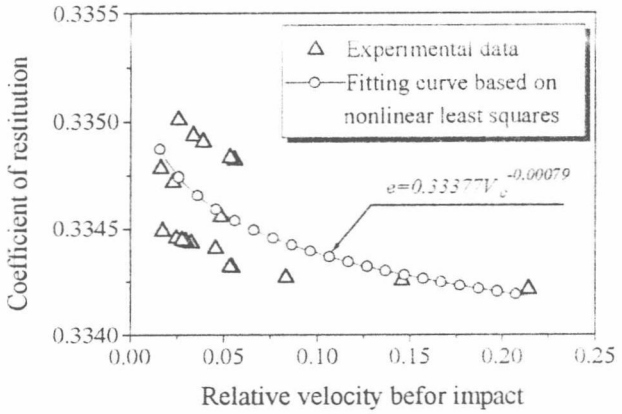

Figure 7. Nonlinear least squares fitting curve based on experimental data

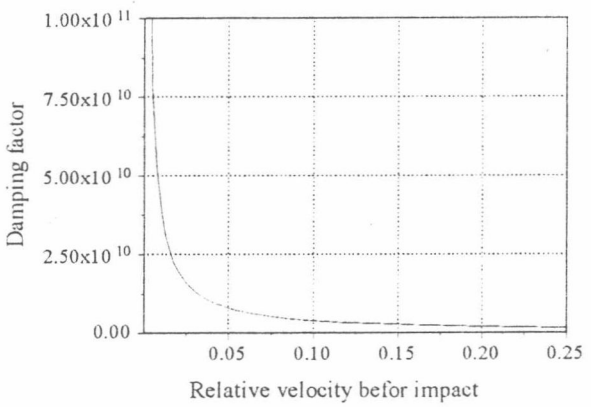

Figure 8. Damping factor versus relative approaching velocity

The second test is to check the identification result of the first test. As shown in Fig. 3, the two beams were moved away from the equilibrium position to positions P_1 and P_2 so that the distance S was 0.06m. Then, the two beams were released and the impact force was recorded as shown in Fig. 9. In order to make a comparison between the measured impact force and the computed one based on the identified damping in the first

test, the sample frequency was set to 20kHz. In the numerical simulation of the impact force, the Young's modules and the Poisson ratio of the steel were chosen as 206Gpa and 0.3, respectively. Figuation 10 shows good agreement of the measured impact force with the computed one on the basis of the identified damping. Figuation 10 also shows that very large error would be produced if the impact damping was not taken into account in numerical simulation.

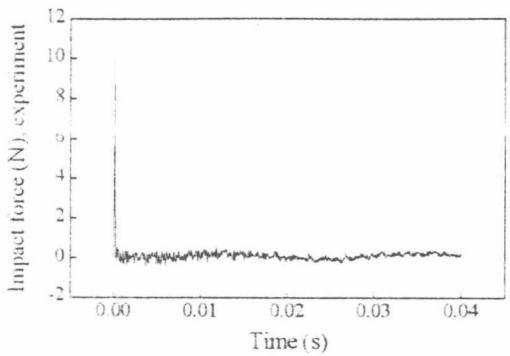

Figure 9. Measured time history of single impact force

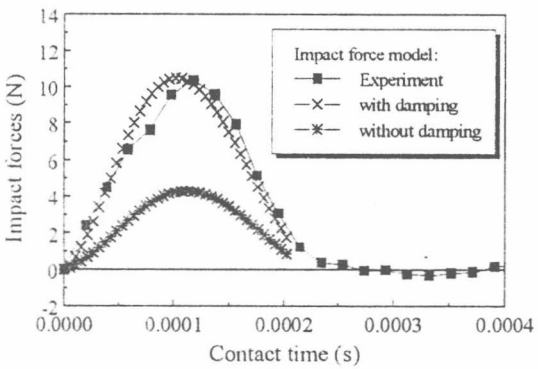

Figure 10. Comparison between experimental and simulated impact forces

5 CONCLUSIONS

The approach proposed in this paper enables one to identify the parameters of the impact damping model of two elastic bodies through the impulse and the maximum of impact force, which can be extracted from the measured time history of the impact force. As two by-products, the coefficient of restitution and the relative approaching velocity of two elastic bodies can be obtained from the impulse and the maximum of impact force so that the efforts to measure these two quantities in current technique can be avoided.

ACKNOWLEDGMENTS

This research was supported by the National Natural Science Foundation of China under Grant Number 957202

REFERENCES

1. Dubowsky S. and Gardner T. N., 1975, "Dynamic interactions of link elasticity and clearance connections in planar mechanical systems". *Journal of Engineering for Industry*, **97B**: 652-661
2. Goldsmith W., 1960, *Impact*, Edward Arnold Ltd., London
3. Hunt K. H. and Crossley F. R. E., 1975, "Coefficient of restitution interpreted as damping in vibroimpact", *Journal of Applied Mechanics*, **7**: 440-445
4. Yigit A. S, Ulsoy A. G. and Scott R. A., 1990, "Spring-dashpot models for the dynamics of a radially rotating beam with impact", *Journal of Sound and Vibration*, **142**: 515-525
5. Yigit A. S., 1994, "The effect of flexibility on the impact response of a two-link rigid-flexible manipulator", *Journal of Sound and Vibration*, **177**: 349-361
6. Lee T. W. and Wang A. C., 1983, "On the dynamics of intermittent-motion mechanisms, part I: Dynamic model and response", *Journal of Mechanisms, Transmissions, and Automation in Design*, **105**: 534-540
7. Lankarani H. M. and Nikravesh P. E., 1994, "Continuous contact force models for impact analysis in multibody systems", *Nonlinear Dynamics*, **5**: 193-20

COMPUTER AIDED DESIGN FOR VIBRATION ISOLATION SYSTEMS WITH DAMPED ELASTIC STOPS

H. Y. Hu and F. X. Wang

Institute of Vibration Engineering, Nanjing University
of Aeronautics and Astronautics, Nanjing, 210016, China

ABSTRACT

From the viewpoint of nonlinear dynamics, a systematic design approach is proposed for the vibration isolation systems with a damped elastic stop. The approach consists of three steps. The first one is to design a slightly damped linear isolation system according to the linear theory of vibration isolation. Then, the optimal parameters for the damped elastic stop can be chosen in a region given according to the singularity analysis of the primary resonance. Finally, the continuation scheme for periodic motion and the interpolated cell-to-cell mapping for the global behavior of the system are used to test and evaluate the design. The approach enables one to make use of damping in the stop to attenuate the resonance transmissibility, while keeping very low transmissibility in the frequency range of vibration isolation.

KEYWORDS: vibration isolation, nonlinear vibration, elastic stop, design, primary resonance

INTRODUCTION

Elastic stops have been widely used to limit the excessive deformation of the elastic component of a vibration isolator in engineering. As reviewed in Hu (1996), no theoretical design approach for this kind of vibration isolators has been reported in archival publications, partially because the combined restoring force of the elastic component and the stop in the vibration isolator is no longer linear with respect to the large deformation. In the current

design of the vibration isolator with an elastic stop, the stiffness and damping of the main elastic component is determined first on the basis of linear theory of vibration isolation. Then, the elastic stop is empirically designed and modified through a series of tests. Such a design procedure is not only very expensive, but also dangerous in the test when the nonlinear dynamics of the vibration isolation system is totally unknown.

The primary aim of this paper is to present a theoretical design approach for the vibration isolation system with a damped elastic stop from the view point of nonlinear dynamics. As the system is piecewise linear, i.e., nonlinear by nature, it is not possible to gain insight into the complicated dynamics of the system by using any analytical approach. Thus, analytical approaches and computational approaches are combined to form a systematic and practical design approach.

MECHANICAL MODEL AND PRIMARY RESONANCE

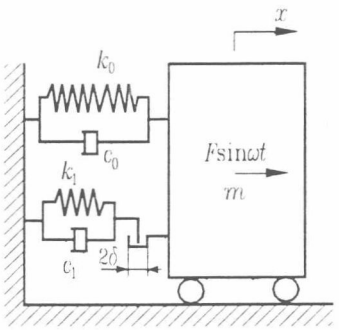

Figure 1: Mechanical model of the vibration isolation system

Consider the vibration isolation system shown in Figure 1, where a damped elastic stop with symmetric clearance is mounted so that the combined restoring force in the system is piecewise linear when $|x|$, the absolute value of the displacement, exceeds the clearance δ. Using the dimensionless time and displacement, as well as a set of dimensionless positive parameters

$$\begin{cases} \tau = \sqrt{\dfrac{k_0}{m}}t, & y = \dfrac{x}{\delta}, & \zeta_0 = \dfrac{c_0}{2\sqrt{mk_0}}, & \zeta_1 = \dfrac{c_1}{2\sqrt{mk_0}}, \\ \mu = \dfrac{k_1}{k_0}, & f = \dfrac{F}{k_0\delta}, & \lambda = \omega\sqrt{\dfrac{m}{k_0}}, \end{cases} \tag{1}$$

one can write out the differential equation of motion of the system

where the dot represents the derivative with respect to the dimensionless time τ and

$$g(y)=\begin{cases} y, & |y|\le 1,\\ (1+\mu)y-\mu\,\mathrm{sgn}(y), & |y|>1; \end{cases} \tag{3}$$

$$h(\dot{y})=\begin{cases} 2\zeta_0\dot{y}, & |y|\le 1,\\ 2(\zeta_0+\zeta_1)\dot{y}, & |y|>1; \end{cases} \tag{4}$$

are the piecewise linear forces of elastic components and damping, respectively.

To provide the theoretical background for the design, it is essential to study the nonlinear primary resonance of the system when $\max|y|>1$. If the parameters ζ_0,ζ_1,μ and f are small, the primary resonance can be approximated, through the use of average approach, as

$$y(\tau)=a(\tau)\cos[\lambda\tau+\varphi(\tau)], \tag{5}$$

where $a(\tau)$ and $\varphi(\tau)$ yield

$$\dot{a}=q(a)-\frac{f}{2\lambda}\cos\varphi,\qquad \dot{\varphi}=\frac{1-\lambda^2}{2\lambda}+\frac{p(a)}{\lambda a}+\frac{f}{2\lambda a}\sin\varphi, \tag{6}$$

$$\begin{cases} p(a)=\dfrac{\mu a}{2\pi}(2\varphi_0-\sin 2\varphi_0),\\ q(a)=\dfrac{a}{\pi}[\xi_0\pi+\xi_1(2\varphi_0-\sin 2\varphi_0)], \qquad \varphi_0=\arccos(\dfrac{1}{a}), \qquad a>1. \end{cases} \tag{7}$$

From Eqn.6, one has the relationship between the amplitude of the steady state resonance and the excitation frequency

$$[p(a)+\frac{a}{2}(1-\lambda^2)]^2+\lambda^2q^2(a)-(\frac{f}{2})^2=0. \tag{8}$$

To classify the types of the primary resonance, one can focus on the case of $a>>1$ and let $z=1/a<<1$. Using the Taylor expansion of order three with respect to z, one obtains the bifurcation equation of the primary resonance from Eqn.8 (see Wang and Hu, 1997)

$$G(z,\eta,\alpha_1,\alpha_2)\equiv[(z-z^3/6)+\eta]^2+\alpha_1^2-\rho\alpha_1^2z+\alpha_2z^2=0, \tag{9}$$

where

$$\alpha_1 = \frac{\pi\lambda\xi_1(1+\sigma)}{2\mu}, \qquad \alpha_2 = [\frac{4\alpha_1}{\pi(1+\sigma)}]^2 - (\frac{\pi f}{4\mu})^2, \tag{10}$$

$$\eta = \frac{\pi}{4}(\frac{\lambda^2-1}{\mu}-1), \qquad \rho = \frac{8}{\pi(1+\sigma)}, \qquad \sigma = \frac{\zeta_0}{\zeta_1}. \tag{11}$$

According to the singularity theory, one can prove that Eqn.9 is a universal unfolding of the normal form $[(z-z^3/6)+\eta]^2$ with two unfolding parameters α_1 and α_2. The transition set of G consists of the following two subsets.

(1) Bifurcation set $B = B_1 \cup B_2 \cup B_3$:

$$B_1: \alpha_1 = 0, \qquad B_2: \alpha_2 = \frac{\rho^2}{4}\alpha_1^2, \qquad B_3: \alpha_2 = \frac{1}{8}[4\rho\alpha_1^2 - 1 \pm \sqrt{1-16\alpha_1^2+8\rho\alpha_1^2}]. \tag{12}$$

(2) Hysteresis set H:

$$H: \alpha_1 = \pm\sqrt{\frac{\alpha_2 z^4 + [\alpha_2 + (1-z^2/2)^2]^2}{(\rho z-1)z^2}}, \qquad \alpha_2 = \frac{1}{2}[-b \pm \sqrt{b^2-4c}], \tag{13}$$

where

$$\begin{cases} b = z^4 + 2(1-\dfrac{z^2}{2})^2 + \dfrac{2(1-\rho z)z}{\rho}(1+\dfrac{z^2}{2}), \\ c = (1-\dfrac{z^2}{2})^3[(1-\dfrac{z^2}{2}) + \dfrac{2(1-\rho z)z}{\rho}]. \end{cases} \tag{14}$$

It can be proved that the hysteresis set H intersects with the bifurcation set B only once at the subset B_3.

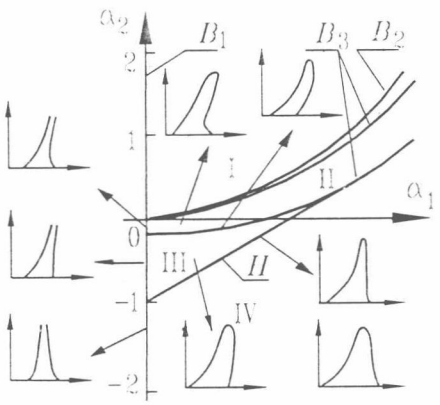

Figure 2: Transition set of G with respect to unfolding parameters α_1 and α_2

Now, one can check the possible types of the primary resonance for $\alpha_1 > 0$, which is the natural consequence of $\zeta_0 > 0$ and $\zeta_1 > 0$ in practice. Figure 2 shows a typical transition set of these two unfolding parameters. The transition set divides the right half plane of (α_1, α_2) into 4 regions as shown in Figure 2. In each region, the amplitude-frequency curve of the primary resonance looks the same qualitatively. This figure, thus, enables one to choose an appropriate combination of unfolding parameters so that the vibration isolation system possesses the desired qualitative behavior in primary resonance.

It should be emphasized at the end of this section that though the above analysis is made for a piecewise linear system on the assumption of weak nonlinearity, i.e., the parameters μ and ζ_1 are small, the numerical simulations in Wang and Hu (1997) showed that the results were valid even when μ and ζ_1 were not small.

DESIGN APPROACH

The basic idea of present approach is to design a linear vibration isolation system with very small damping first, and then an elastic stop with large damping. In the working frequency range, the slightly damped vibration isolation system has required vibration transmissibility. Once the vibration isolation system undergoes the primary resonance somehow, both the elastic stop and the large damping reduce the vibration amplitude and remove the jumping phenomenon that may occur for a harmonically forced nonlinear oscillator.

3.1 *Design of primary system*

The vibration isolation system without any stop is referred to as the primary system hereinafter for brevity. The vibration transmissibility of the primary system yields

$$T = \sqrt{\frac{1+(2\xi_0\lambda)^2}{(1-\lambda^2)^2+(2\xi_0\lambda)^2}}, \tag{15}$$

where only two dimensionless parameters λ and ζ_0 are to be designed. For a linear vibration isolation system in traditional sense, the vibration transmissibility in resonance can only be attenuated by increasing the damping ratio ζ_0. For the vibration isolation system with an elastic stop, however, the task of attenuating the vibration transmissibility in the case of resonance can be left to the damped stop. Hence, a very small damping ratio ζ_0 can be chosen in the design of primary system in order to avoid the system impacting the stop when the system starts running, see Hu (1996). In the case of $\zeta_0 < 0.1$ and $\lambda > 2$, the stiffness of the main elastic component can be determined by using the following approximation of Eqn.15

$$\lambda \geq \sqrt{1+1/T}\ . \tag{16}$$

3.2 *Design of Damped Elastic Stop*

3.2.1 *Preliminary Design*

Given the dimensionless excitation frequency λ, the damping ratios ζ_0 and ζ_1, the system parameters to be designed are only μ and f. These two parameters appear in the expressions of unfolding parameters α_1 and α_2, and hence, follow the selection of the two unfolding parameters. In principle, any parameter combination of α_1 and α_2 in region IV in Figure 2 makes sure that the frequency-amplitude curve of primary resonance does not have jumping. Thus, an arbitrary combination of (α_1, α_2) in region IV can be chosen to determine the corresponding parameters μ and f, provided that the vibration transmissibility is acceptable.

A great number of numerical simulations showed that the stiffness ratio μ should not be too large. As shown in Figure 3, the function of stop is very obvious in the lower frequency range. The response amplitude goes down very rapidly in the beginning of the increase of μ, and then changes not very much later until very complicated dynamics happens. For the sinusoidal excitation of high frequency, the response amplitude has a peak as shown in Figure 4. It is smaller than the initial value only when μ is very large. As a result, an excessive stiffness ratio μ is harmful.

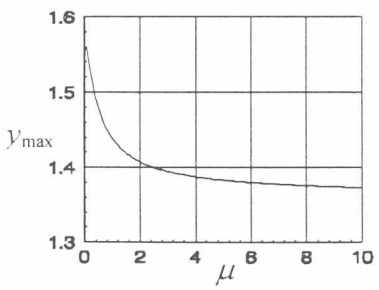

Figure 3: Maximal displacement versus stiffness ratio when $\lambda = 0.5$

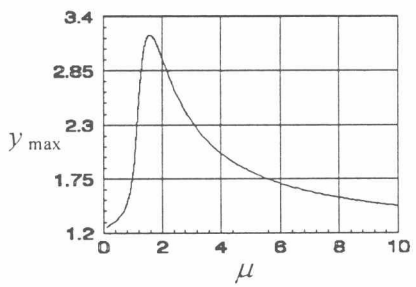

Figure 4: Maximal vibration amplitude versus stiffness ratio when $\lambda = 1.4$

Moreover, the dimensionless excitation amplitude f defined in Eqn.1 is inversely proportional to the clearance δ when the excitation amplitude F is fixed. So, the clearance δ can be determined from α_2. If the clearance is too large, the stop can not be in function. If too small, the vibration may become nonlinear and then undergoes a sub-harmonic resonance in working frequency range.

In summary, the stiffness of the stop should not be very large and the clearance should be appropriate. So, it is necessary to optimize these two parameters, or namely two unfolding parameters in region IV in Figure 2.

3.2.2 *Optimization for Parameters*

Now f, the dimensionless excitation amplitude, is taken as the design variable to look for the minimal stiffness ratio of an elastic stop such that the requirement for vibration transmissibility in the primary resonance is met. The constraint conditions for this problem are as follows:

(a) the parameter boundary where the forced vibration of the system is linear in the working frequency range;

(b) the minimal stiffness ratio of the stop for given resonance transmissibility at different excitation amplitudes (or clearances);

(c) the hysteresis set H that guarantees no jumping and no hysteresis in the primary resonance.

It is obvious that condition (c) has been given in Eqn.13. Hence, only the first two conditions are discussed hereafter.

By eliminating μ in the expressions of α_1 and α_2 in Eqn.10, one obtains

$$\alpha_2 = \frac{64\lambda^2\zeta_1^2 - \pi^2 f^2}{4\pi^2\lambda^2\zeta_1^2(1+\sigma)^2}\alpha_1^2 . \tag{17}$$

The forced vibration of the system in the working frequency range is linear if the following inequality holds true

$$f < f_{\max} \equiv \sqrt{(1-\lambda_w{}^2)^2 + (2\xi_0\lambda_w)^2} , \tag{18}$$

where λ_w is the ratio of working frequency to the natural frequency of the primary system. Given $f_{\max}$, the critical value of Eqn.18, a parabola denoted by $f_{\max}$ in Figure 5(b) can be determined from Eqn.17. This is the parameter boundary of condition (a).

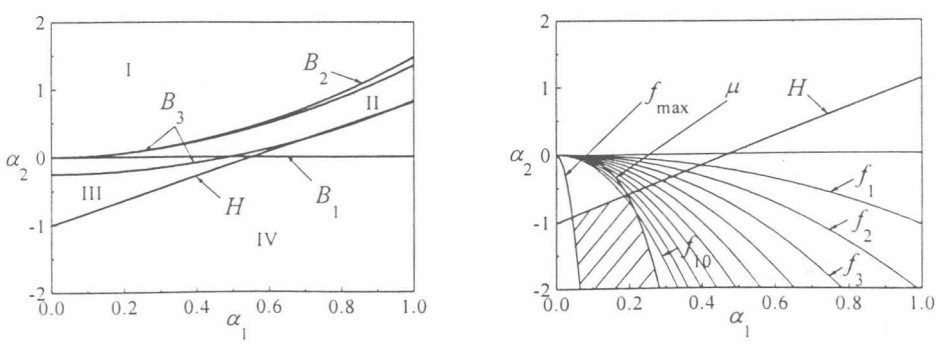

(a) Transition set of unfolding parameters (b) Optimal parameter region

Figure 5: Transition set and optimal parameter region in (α_1, α_2) plane when $\zeta_0 = 0.01$, $\zeta_1 = 0.2$, $\lambda_w = 2.75$ and $a_a = 1.2$ at $f = 0.52$